0026-895X/06/6905-1542–1553$20.00
MOLECULAR PHARMACOLOGY
Vol. 69, No. 5
18945/3104811
Mol Pharmacol 69:1542–1553, 2006
Printed in U.S.A.

Electrophysiological Characterization and Modeling of the Structure Activity Relationship of the Human Concentrative Nucleoside Transporter 3 (hCNT3)

Huankai Hu, Christopher J. Endres, Cheng Chang, Nagavedi S. Umapathy, Eun-Woo Lee, You-Jun Fei, Shirou Itagaki, Peter W. Swaan, Vadivel Ganapathy, and Jashvant D. Unadkat

Department of Biochemistry and Molecular Biology, Medical College of Georgia, Augusta, Georgia (H.H., N.S.U., Y-J.F., S.I., V.G.); Department of Pharmaceutical Sciences, University of Maryland, Baltimore, Maryland (C.C., P.W.S.); and Department of Pharmaceutics, University of Washington, Seattle, Washington (C.J.E., E-W.L., J.D.U.)

Received September 28, 2005; accepted January 30, 2006

ABSTRACT

We characterized the electrophysiology, kinetics, and quantitative structure-activity relationship (QSAR) of the human concentrative nucleoside transporter 3 (hCNT3) expressed in *Xenopus laevis* oocytes by measuring substrate-induced inward currents using a two-microelectrode voltage-clamp system. At membrane potentials between −30 and −150 mV, sodium activation of gemcitabine transport was sigmoidal, with a $K_{0.5}$ of 8.5 ± 0.3 mM for Na^+ and a Hill coefficient of 2.2 ± 0.25 independent of membrane potential. We measured the I_{max} and $K_{0.5}$ for substrate at −50 mV for the nucleoside analog drugs gemcitabine (638 ± 58 nA, 59.7 ± 17.5 μM), ribavirin (546 ± 37 nA, 61.0 ± 13.2 μM), AZT (420 ± 4 nA, 310 ± 9 μM), and 3-deazauridine (506 ± 30 nA, 50.8 ± 9.90 μM). $K_{0.5}$ and I_{max} for substrate were dependent on membrane potential (both increasing as the membrane became more hyperpolarized) for all four drugs. hCNT3 also exhibited pre–steady-state currents. The quantitative structure-activity relationship (QSAR) was examined using comparative molecular field analysis and comparative molecular similarity indices analysis of the inward currents induced by 27 nucleoside analogs with substitutions at both the ribose and the nucleobase. Two statistically significant QSAR models identified electrostatic interaction as the major force in hCNT3 transport and attributed a critical role to the 3′-hydroxyl position of hCNT3 substrates. Steric hindrance at the 3-position and positive charge at the 5-position of the pyrimidine ring were favorable for transport. Two hCNT3 pharmacophore models revealed the minimal features required for hCNT3 transport as two hydrogen bond acceptors at 3′-OH and 5′-O and the hydrophobic center occupied by the base ring.

Nucleosides and nucleoside drugs are typically polar molecules that do not readily diffuse across biological membranes. Therefore, the entry of these compounds into cells is mediated by nucleoside transport proteins. These transporters are present in the plasma membrane and intracellular membranes (Mangravite et al., 2003; Baldwin et al., 2004; Gray et al., 2004; Kong et al., 2004) and are important in the salvage pathway of nucleotide biosynthesis, the action of the physiological regulator adenosine and the absorption and disposition of nucleoside drugs such as ribavirin (Jarvis et al., 1998; Patil et al., 1998) and gemcitabine (Mackey et al., 1998).

Nucleoside transporters can be classified into two broad groups based on their energy requirements. The concentrative nucleoside transporters (CNTs) are symporters. Their energy source is derived from the cotransport of sodium down its electrochemical gradient. The equilibrative or facilitative nucleoside transporters (ENTs) are sodium-independent and transport nucleosides and nucleoside analogs down their concentration gradient. Three human CNTs have now been cloned that correspond to the functionally characterized CNTs [hCNT1 (cit), hCNT2 (cif), and hCNT3 (cib)]. Some evidence suggestd that the cs and csg-type transporters may be functional variants of these three CNTs (Lai et al., 2005). hCNT3 has broad substrate specificity, accepting both pu-

This work was supported by National Institutes of Health grants HD44404 (to V.G.), GM54447 (to J.D.U.), DK56631 (to P.W.S.), and GM07750 (C.J.E.).
Article, publication date, and citation information can be found at http://molpharm.aspetjournals.org.
doi:10.1124/mol.105.018945.

ABBREVIATIONS: CNT, concentrative nucleoside transporter; ENT, equilibrative nucleoside transporter; MES, 2-(*N*-morpholino)ethanesulfonic acid; AZT, azidothymidine; CoMFA, comparative molecular field analysis; CoMISA, comparative molecular similarity indices analysis; QSAR, quantitative structure-activity relationship; 3D, three-dimensional.

rines and pyrimidines as substrates (Ritzel et al., 2001). In contrast, hCNT1 preferentially transports pyrimidines, whereas hCNT2 preferentially transports purines.

Nucleoside transporters are important in the disposition, efficacy and toxicity of various nucleoside drugs. For example, they play an important role in mediating entry of polar anticancer drugs into tumor cells such as gemcitabine and 5-fluorouridine (Mackey et al., 1998; Mata et al., 2001). Thus, it is not surprising that variability in the expression of these transporters modulates the efficacy and toxicity of anticancer nucleoside drugs (Huang et al., 2004). In addition, nucleoside transporters are important in mediating cytotoxicity of nucleoside antiviral drugs (Jarvis et al., 1998; Lai et al., 2004). Therefore, for future development of nucleoside drugs, it is important to determine the molecular requirements of nucleoside transporters.

We have characterized the molecular requirements of hCNT1, hCNT2 (Patil et al., 2000), and hENT1 (Lum et al., 2000) by developing pharmacophore models for these three transporters (Chang et al., 2004). Herein, we report in detail the electrophysiology and substrate specificity of hCNT3 expressed in *Xenopus laevis* oocytes using a two-microelectrode voltage-clamp system. By measuring the substrate-induced inward currents, we were able to directly characterize the transport kinetics of a number of drugs (such as azidothymidine, ribavirin, and gemcitabine) and nucleoside analogs. Using these data, we have elucidated the qualitative molecular requirements of hCNT3 transport by generating both a QSAR model and a pharmacophore model for the transporter. Then, we compared and contrasted these models with those previously generated by us for hCNT1, hCNT2 and hENT1 (Chang et al., 2004).

Materials and Methods

Materials and Reagents. All nucleosides and nucleoside analogs were purchased from Sigma-Aldrich (St. Louis, MO).

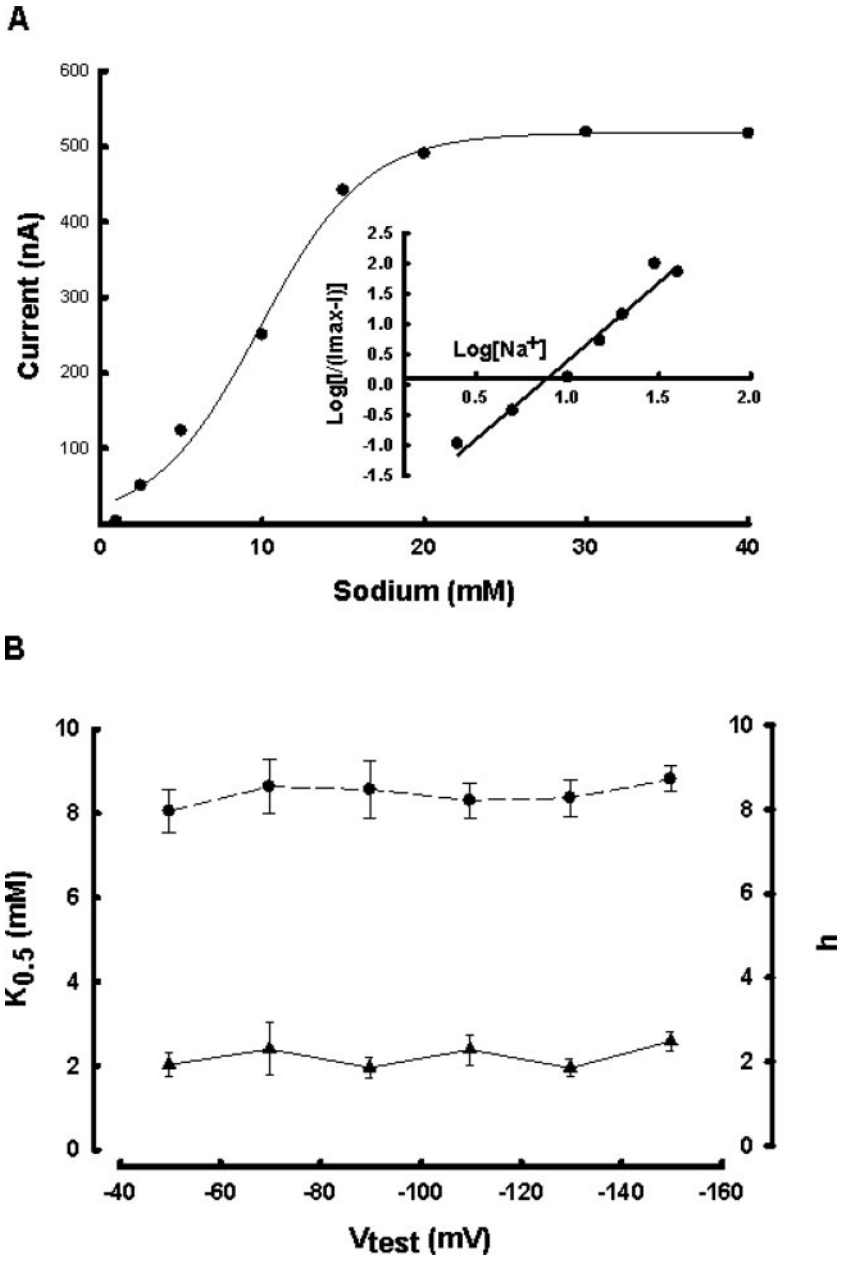

Fig. 1. Na^+ activation kinetics of gemcitabine transport by hCNT3 expressed in *X. laevis* oocytes. The sodium-activation kinetics of gemcitabine transport by hCNT3 were examined at various membrane potentials using 250 μM gemcitabine as the substrate. A, a representative dataset of the substrate-induced inward current as a function of Na^+ concentration (1–40 mM) measured at −50 mV. The solid line is the nonlinear regression fit of the Hill equation to the data, which was confirmed by linear regression (inset). B, estimates of both h (▲, solid line) and $K_{0.5}$ (●, dashed line) were determined by nonlinear regression analysis of the kinetic data at various membrane potentials according to the Hill equation (−50 to −150 mV). Both $K_{0.5}$ and h were independent of membrane potential over this range of membrane potential. The parameter estimates of h suggest a Na^+/gemcitabine translocation ratio of 2.

Cloning and Functional Expression of hCNT3 in *X. laevis* Oocytes. Full-length hCNT3 was cloned from a human intestinal cDNA library. The coding region of the clone was amplified by polymerase chain reaction and subcloned into the oocyte expression vector pGH19 (kindly provided by Dr. Peter S. Aronson, Yale University, New Haven, CT). Capped cRNA from the cloned hCNT3 cDNA was then synthesized using the mMESSAGE mMACHINE kit (Ambion, Austin, TX) according to the manufacturer's protocol. Mature oocytes from *X. laevis* were isolated, treated with collagenase A (1.6 mg/ml), manually defolliculated, and maintained at 18°C in modified Barth's medium supplemented with 10 mg/l gentamicin (Parent et al., 1992). On the following day, oocytes were injected with 50 ng of cRNA. Oocytes injected with water served as controls. The oocytes were used for electrophysiological studies 6 days after cRNA injection. Electrophysiological studies were performed by the conventional two-microelectrode voltage-clamp method (Loo et al., 1993; Mackenzie et al., 1996a,b). Oocytes were perfused with a NaCl-containing buffer (100 mM NaCl, 2 mM KCl, 1 mM MgCl2, 1 mM CaCl2, 3 mM HEPES, 3 mM MES, and 3 mM Tris, pH 7.4) followed by the same buffer containing different nucleosides or in the same buffer containing different nucleoside analogs dissolved in 0.5% dimethyl sulfoxide. The membrane potential was held steady at −50 mV.

For studies on the Na^+ dependence of substrate-induced currents, the oocytes were perfused with buffer containing increasing concentrations (1–40 mM) of Na^+ and 250 μM gemcitabine (0.5% dimethyl sulfoxide), and the substrate-induced inward currents were measured. All subsequent studies were conducted at saturating (100 mM) Na^+ concentrations.

For the kinetic and current-voltage relationship studies, step changes in membrane potential were applied, for durations of 100 ms in 20-mV increments between −30 and −150 mV in the presence of increasing concentrations of substrates.

Pre–Steady-State Currents. A pulse protocol was used in electrophysiology studies as described previously (Loo et al., 1993; Boorer et al., 1994; Panayotova-Heiermann et al., 1995; Mackenzie et al., 1996b). Oocytes expressing hCNT3 (or water-injected control oocytes) were constantly perfused with a standard solution containing 100 mM NaCl or 100 mM *N*-methyl-D-glutamate chloride, pH 7.5. Oocytes were held at −50 mV (membrane holding potential, V_h), and

TABLE 1

Electrophysiological characterization of natural nucleosides by hCNT3 expressed in *X. laevis* oocytes

The kinetic parameters I_{max}, $K_{0.5}$, and the ratios of the two ($I_{max}/K_{0.5}$) for various naturally occurring nucleosides were determined by measuring the substrate-induced inward currents at increasing substrate concentrations (1 μM to 1 mM). The membrane potential was held at −50 mV. The parameters are a mean ± S.E. of three independent measurements.

Substrate	I_{max}	$K_{0.5}$	$I_{max}/K_{0.5}$
	nA	μM	*nA* / μM
Uridine	171.3 ± 6.2	13.3 ± 1.9	12.9
Cytidine	184.2 ± 5.6	15.8 ± 1.8	11.7
Thymidine	235.7 ± 8.9	19.1 ± 3.0	12.3
Adenosine	238.5 ± 13.4	17.8 ± 4.2	13.4
Inosine	391.3 ± 14.4	31.3 ± 4.3	12.5
Guanosine	326.0 ± 11.5	27.2 ± 3.7	11.9

TABLE 2

Chemical structure of nucleoside analogs

n	Name	Base					Sugar		
		X	Y	R_1	R_2	R_3	R_4	R_5	R_6
	Purines								
1	Adenosine								
2	2′-Deoxyadenosine			H	NH_2	H	H	OH	OH
3	2′-3′-Dideoxyadenosine			H	NH_2	H	H	H	OH
4	5′-Deoxyadenosine			H	NH_2	H	OH	OH	H
5	1-Methyladenosine[a]			H	$=NH_2$	H	OH	OH	OH
6	Inosine								
7	2′-Deoxyinosine			H	OH	H	H	OH	OH
8	2′-3′-Dideoxyinosine (ddI)			H	OH	H	H	H	OH
9	Guanosine								
10	2′-Deoxyguanosine			NH_2	=O	H	H	OH	OH
11	8-Bromoguanosine			NH_2	=O	Br	OH	OH	OH
12	Ribavirin[b]						OH	OH	OH
	Pyrimidines								
13	Uridine								
14	2′-Deoxyuridine	N	C	O	H	H	H	OH	OH
15	3′-Deoxyuridine	N	C	O	H	H	OH	H	OH
16	2′-3′-Didexoyuridine	N	C	O	H	H	H	H	OH
17	5-Fluorouridine	N	C	O	F	H	OH	OH	OH
18	5-Fluoro-5′-deoxyuridine	N	C	O	F	H	OH	OH	H
19	5-Bromouridine	N	C	O	Br	H	OH	OH	OH
20	5-Bromo-2′-deoxyuridine	N	C	O	Br	H	OH	OH	OH
21	5-Iodouridine	N	C	O	I	H	OH	OH	OH
22	5-Iodo-2′-deoxyuridine	N	C	O	I	H	H	OH	OH
23	3-Deazauridine	C	C	O	H	H	OH	OH	OH
24	6-Azauridine	N	N	O	H	H	OH	OH	OH
25	Cytidine								
26	2′-Deoxycytidine	N	C	NH_2	H	H	H	OH	OH
27	3′-Deoxycytidine	N	C	NH_2	H	H	OH	H	OH
28	2′-3′-Dideoxycytidine	N	C	NH_2	H	H	H	H	OH
29	2′-2′-Diflouro-2′-deoxycytidine (Gemcitabine)	N	C	NH_2	H	F	F	OH	OH
30	Thymidine								
31	2′,5′-Dideoxythymidine	N	C	O	CH_3	H	H	OH	H
32	3′-Azido-3′-deoxythymidine (AZT)[c]	N	C	O	CH_3	H	H	NNN[c]	OH
33	2′-3′-Didehydroxy-2′3′-deoxythymidine (Stavudine)[d]	N	C	O	CH_3			H	OH

[a] 1-Methyladenosine has a methyl group at N1 and the double bond between N1 and C6 is shifted to between C6 and R_2.
[b] Ribivirin has a 1,2,4-triazole-3-carboxamide group at C1′ instead of a pyrimidine group.
[c] AZT has an azido group at C3′.
[d] Stavudine has a double bond between the 2′ and 3′ carbons.

membrane currents were measured after stepping from V_h to testing potentials (V_t,) for 100 ms, between −150 and +50 mV in 20-mV increments. The currents were averaged from three sweeps. Currents were filtered at 500 Hz and digitized at a frequency of 100 ps/point.

Data Analysis of Electrophysiological Measurements. Electrophysiological measurements of substrate-induced currents were repeated at least three times with separate oocytes. The substrate-induced currents in water-injected oocytes were negligible and subtracted from those in hCNT3-expressing oocytes. The data are presented as mean ± S.E.M. of these replicates unless otherwise noted.

Na^+ activation or saturation kinetics for substrate-induced currents were studied by monitoring the currents at increasing concentrations of Na^+ or substrates using the model $I = I_{max} \times [C^h/(C^h + K_{0.5}^h)]$, where I is substrate-induced current, C is the Na^+ or substrate concentration, I_{max} is the current induced by the maximal Na^+ or substrate concentration, $K_{0.5}$ is the concentration at which half-maximal I_{max} was observed, and h is the Hill coefficient. The above model was fit to the data using nonlinear least-squares regression using SigmaPlot (SPSS Inc., Chicago, IL) and confirmed by linear regression of Eadie-Hofstee or Hill plots.

Pre–steady-state currents were analyzed using pClampex and pClampfit (Molecular Devices, Sunnyvale, CA) and SigmaPlot. Pre–steady-state or transient currents (I_2) with a relaxation time constant τ_2 as a result of the expression of hCNT3 were isolated from the total current (I_t) recorded during the jumping protocol by a fitted method according to a standard exponential decay equation: $I_t = I_1 e^{-1/\tau_1} + I_2 e^{-1/\tau_2} + I_{ss}$, as described previously (Loo et al., 1993; Boorer et al., 1994; Panayotova-Heiermann et al., 1995; Mackenzie et al., 1996b). The capacitive (I_1) with a relaxation time constant $\tau 1$ and steady-state (I_{ss}) currents were subtracted from the total current (I_t) to derive the pre–steady-state or transient currents (I_2) because of the expression of hCNT3. The charge (Q) translocation associated with hCNT3 expressed in oocytes was obtained by integration of the pre–steady-state currents (I_2) with the time at each testing membrane potential, and charge movements were fitted to the Boltzmann equation, $[(Q - Q_{hyp})/Q_{max}] = (1/[1 + e^{z(V_t - V_{0.5})F/RT}])$, where $Q_{max} = Q_{dep} - Q_{hyp}$. Q_{dep} and Q_{hyp} represent Q at depolarizing and hyperpolarizing limits, z is the apparent valence of the movable charge, $V_{0.5}$ is the testing membrane potential for 50% charge translocation, F is Faraday's constant, R is the gas constant, and T is the absolute temperature.

Pharmacophore Modeling. A pharmacophore is the representation of the spatial arrangement of structural features that are required for a certain biological activity. The model can give insight into the transport process, form a basis for the design of more active compounds, and assist the identification of other molecules that contain the same pharmacophore. Two widely applied programs, GASP (Jones et al., 1995) and DISCOtech (Martin et al., 1993), were used for hCNT3 pharmacophore model identification. Both programs can generate pharmacophore models containing site features, which are proposed features from the transporter that interact with the substrate. They both require the input of the most active and structurally diverse substrates, based on which 2-deoxycytidine, 5-deoxyadenosine, 5-iodouridine, guanosine, and inosine were selected for model generation.

GASP Algorithm. GASP (Genetic Algorithm Similarity Program) is a genetic algorithm developed for the perception of pharmacophore models by superposition of sets of flexible molecules (Jones et al., 1995). GASP attempts to optimize the orientation and conformation of molecules by quickly and efficiently fitting them to similarity constraints. When generating the alignment, to broaden the diversity of conformations that are considered, the "population size" is increased to 125 and the "allele mutate weight" to 96. With increased population size and mutation rate, conformations with more diversity are generated. To avoid possible convergence issues due to the increased mutation rate, the convergence criteria were loosened by increasing the "fitness increment" to 0.02. A total of 10 pharmacophore models were generated, and the optimal model was selected based on visual inspection.

DISCOtech Algorithm. DISCOtech is an enhanced version of the program DISCO (DIStance COmparisons), which generates pharmacophore models using a clique detection algorithm to find the common geometrical placement of structural points among all active compounds. The parameter settings were implemented as described previously (Chang et al., 2004).

Comparative Molecular Field Analysis. CoMFA has been applied with considerable success in drug design and transport analyses (Horwitz et al., 1994; Swaan et al., 1997; Kroemer et al., 1998; Schaal et al., 2001). In this approach, the gradual changes in observed biological properties can be explained by evaluating the electrostatic (coulombic) and steric (van der Waals) interaction fields at regularly spaced grid points surrounding a set of mutually aligned hCNT3 substrates. The structures of 33 compounds with measured transport activities were sketched in Sybyl 6.9, and Gasteiger-Marsili charges were assigned. All structures were optimized using the Tripos force field with a distance-dependent dielectric coefficient and the Powell conjugated gradient algorithm with an energy change convergence criterion of 0.001 kcal/mol. Because of the similarity of structure backbones, all structures were aligned using the simple "Fit Atom" command in Sybyl so that the backbones (sugar ring and base ring) are superimposed onto each other. CoMFA calculations were performed based on the aligned 33 molecules (Fig. 7A) as described previously (Chang et al., 2004). The inward current (in nanoamperes) measured at 10 μM ($I_{10\ \mu M}$) as well as log $I_{10\ \mu M}$ were used in the analyses to represent transporter activity for each compound. At low substrate concentrations (10 μM), it is safe to assume that the current is proportional to transport rate (V_{max}/K_m), because the substrate concentration is less than typical nucleoside K_m values (uridine, thymidine, cytidine, adenosine, guanosine, and inosine), which range between 10 and 30 μM.

Comparative Molecular Similarity Indices Analysis. The CoMSIA algorithm is an extension of CoMFA methodology that differs in the implementation of the fields. Whereas CoMFA calculates steric fields using a Lennard-Jones potential and electrostatic

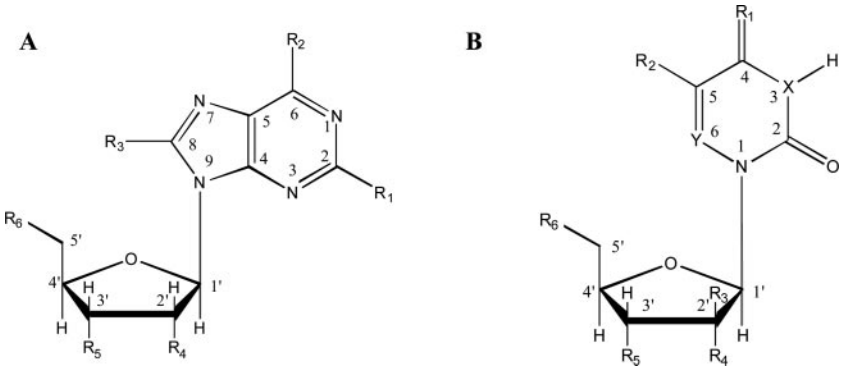

Fig. 2. Chemical structure of nucleoside analogs. The chemical structure of the purine and pyrimidine nucleoside analogs used in the structure-activity experiments. The functional group substitutions are explained in Table 2.

fields using a Coulombic potential, CoMSIA implements a Gaussian type function to avoid the extreme values commonly generated by the other algorithms. The Gaussian function also results in smoother, less fragmented surfaces in the final model representation. In addition, the algorithm allows the correlation between substrate transport activity and either steric, electrostatic, hydrophobicity, H-bond acceptor, or H-bond donor field surrounding the molecule. Different field values are calculated using the Gaussian function. Using the set of superimposed substrates described above, the CoMSIA algorithm was implemented as described previously (Chang et al., 2004).

Results

Sodium Activation Kinetics for Gemcitabine. We examined the sodium activation kinetics of hCNT3 after its functional expression in *X. laevis* oocytes. The inward current induced by gemcitabine (250 μM) was dependent on Na^+ concentration (Fig. 1A). The Na^+-current relationship was sigmoidal, indicating the involvement of more than one Na^+ in the activation process. Analysis of the data according to the Hill equation gave a value of 8.5 $\pm$ 0.3 mM for $K_{0.5}$ for

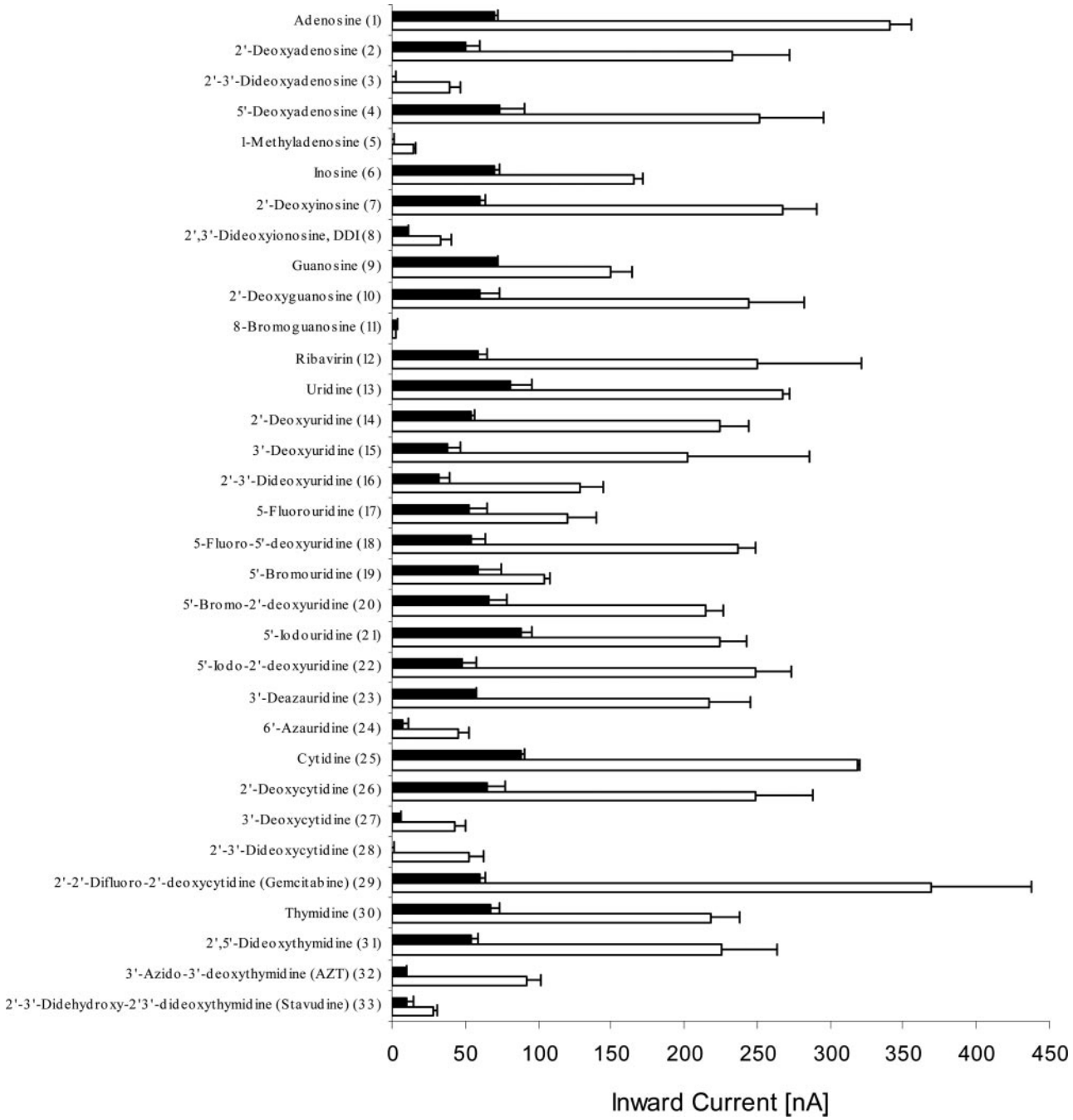

Fig. 3. Purine and pyrimidine nucleoside substrate profile of hCNT3. The inward currents induced by different nucleosides and nucleoside analogs (10 μM, solid bar; 100 μM, open bar) in oocytes expressing human CNT3. Oocytes were injected with human CNT3 cRNA, and 6 days after injection, they were used in electrophysiological studies. The oocytes were perfused with a NaCl-containing buffer followed by the same buffer containing different nucleoside derivatives. The membrane potential was held steady at -50 mV and the currents were recorded. Data (means $\pm$ S.E.M.) are from three independent measurements.

Na^+ and 2.2 ± 0.3 for h. These two parameters were not influenced by membrane potential (Fig. 1B). These data show that the transport of gemcitabine by hCNT3 occurs with a Na^+/gemcitabine stoichiometry of 2:1 and that the Na^+ activation kinetics are independent of membrane potential.

Transport for Natural Nucleosides. We investigated in detail the kinetics for the transport of six naturally occurring nucleosides by hCNT3 using the *X. laevis* oocyte expression system. The transport function was monitored as substrate-induced inward currents in the presence of Na^+. We determined the $K_{0.5}$ and I_{max} values for the pyrimidine nucleosides uridine, cytidine, and thymidine and the purine nucleosides adenosine, inosine, and guanosine at −50 mV membrane potential (Table 1). All substrates exhibited high affinity, with $K_{0.5}$ values in the low micromolar range (13–31 μM). These data are consistent with those published previously (Toan et al., 2003; Zhang et al., 2003). The purine nucleosides generally have higher transport capacity and lower affinity than the pyrimidine nucleosides, but the magnitude of this difference is 2-fold or less, and the transport rates ($I_{max}/K_{0.5}$) for all six substrates averaged 12.5 nA/μM and did not vary by more than 5%.

Substrate Selectivity and Specificity of Nucleobase and Ribose Substitutions. To determine the substrate specificity and elucidate the structure-activity relationship of hCNT3, we determined the inward current induced by both low (10 μM) and high (100 μM) concentrations of 27 nucleoside analogs (either purines or pyrimidines; Table 2 and Fig. 2) with substitutions on the nucleobase, the ribose moiety, or both. These compounds represent a broad array of nucleoside analogs and include substitutions of various functional groups. The inward current induced by each substrate was determined in *X. laevis* oocytes expressing hCNT3 (Fig. 3). At 100 μM, gemcitabine, 2′-deoxyinosine, 5′-deoxyadenosine, ribavirin, 5′-iodo-2′-deoxyuridine, and 2′-deoxycytidine (compounds 29, 7, 4, 12, 22, and 26, respectively) were, in rank order, the nucleoside analogs that induced the greatest inward current, suggesting that these compounds are relatively good substrates of hCNT3. In contrast, 8-bromoguanosine, 1-methyladenosine, and stavudine (compounds 11, 5, and 33, respectively) had negligible induced inward currents, suggesting that these compounds are relatively poor hCNT3 substrates.

In general, nucleoside analogs with substitutions at the 3′-position (3′-deoxy nucleosides) exhibit reduced rate of transport compared with those with substitutions at the 2′-position. For example, 2′-deoxyadenosine (compound 2), 2′deoxyinosine (compound 7), and 2′-deoxycytidine (compound 26) all induced substantially greater currents at 100 μM than their 2′,3′-dideoxy counterparts (compounds 3, 8, and 28, respectively). In contrast, 3′-deoxyuridine and 2′,3′-dideoxyuridine (compounds 15 and 16, respectively) induced inward currents that were comparable with that induced by 2′-deoxyuridine (compound 14), suggesting that, for uridine analogs, the 3′-hydroxyl position is not as critical for substrate translocation as in adenosine, inosine or cytidine analogs.

Transport Kinetics for Antiviral and Anticancer Nucleosides. We also investigated in detail the electrophysiology and kinetics of four nucleoside analogs that are currently used therapeutically: gemcitabine (cytidine analog), ribavirin (guanosine analog), AZT (thymidine analog), and 3-deazauridine (uridine analog). The kinetics of 2′,3′-dideoxyinosine (inosine analog) was not determined because of the low activity. Plots of substrate concentration versus normalized maximal inward current (I/I_{max}) are shown for gemcitabine, ribavirin, AZT, and 3-deazauridine (Fig. 4, A, B, C, and D, respectively). Normalization to the maximal current in each oocyte was done because of the variability in the magnitude of substrate-induced currents in different oocytes because of variable expression levels of the transporter. All four substrates exhibited Michaelis-Menten-type kinetics.

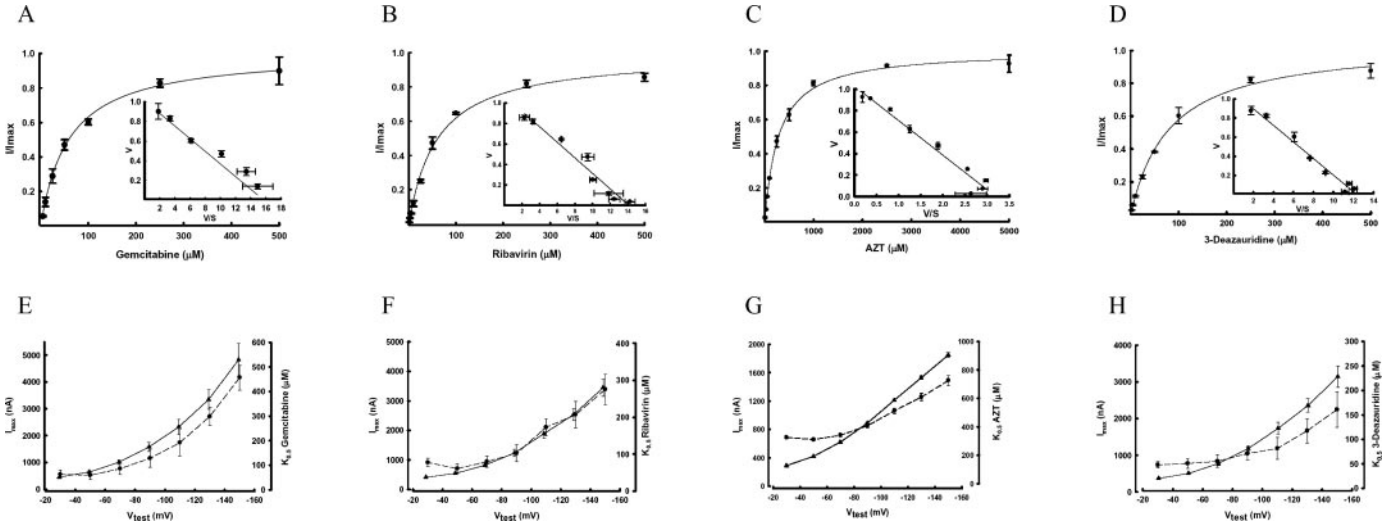

Fig. 4. Kinetics of transport of nucleoside analogs by hCNT3 expressed in *X. laevis* oocytes. The kinetics and membrane potential dependence of I_{max} and $K_{0.5}$ of gemcitabine, ribavirin, AZT, and 3-deazauridine were determined in *X. laevis* oocytes expressing hCNT3. Representative plots of the I/I_{max} ratio at various substrate concentrations for gemcitabine (5–500 μM; A), ribavirin (5–500 μM; B), AZT (5 μM to 5 mM; C), and 3-deazauridine (2.5 to 500 μM; D) are shown as a function of substrate concentration when measured at −50 mV. The solid line is the nonlinear regression fit of the Hill equation to the data. The inset is the linear regression analysis of the same data (Eadie-Hofstee plot). The dependence of I_{max} and $K_{0.5}$ on membrane potential was also determined. The parameter estimates of I_{max} (▲, solid line) and $K_{0.5}$ (●, dashed line) at −30 to −150 mV for gemcitabine (E), ribavirin (F), AZT (G), and 3-deazauridine (H) are plotted as a function of membrane potential. For all substrates, both I_{max} and $K_{0.5}$ were dependent on membrane potential. The data represent the mean ± S.E.M. of three independent measurements in three different oocytes.

The kinetic parameters $K_{0.5}$ and I_{max} were determined by nonlinear regression and confirmed by linear regression (Eadie- Hofstee analysis). At physiologic membrane potential (−50 mV), the affinity of all four compounds was generally lower (51–310 μM) than the affinities of naturally occurring nucleosides (Table 3). Except for AZT, the transport rates ($I_{max}/K_{0.5}$) under nonsaturating conditions were comparable with those of the natural nucleosides (9.0–10.7 nA/μM). In contrast, the $I_{max}/K_{0.5}$ for AZT was approximately 10-fold lower (1.4 nA/μM). Both the affinity ($K_{0.5}$) and I_{max} were dependent on membrane potential for all four compounds examined (Fig. 4, E–H). As the membrane potential hyperpolarized, the affinity decreased (increase in $K_{0.5}$) and the I_{max} increased in an exponential manner. The magnitude of the increase in I_{max} and decrease in affinity (increase in $K_{0.5}$) was greatest for gemcitabine (11-fold from −30 to −150 mV) and the least for AZT (6-fold from −30 to −150 mV). It seems, therefore, that membrane hyperpolarization alters the transport process for all these four substrates from a relatively high-affinity, low-capacity transport to a low-affinity, high-capacity transport.

TABLE 3

Kinetics of transport of nucleoside drugs by hCNT3 expressed in *X. laevis* oocytes

The kinetic parameters I_{max}, $K_{0.5}$, and ratio of the two ($I_{max}/K_{0.5}$) of four nucleoside analog drugs were determined by measuring the substrate-induced inward currents at increasing substrate concentrations (1 μM to 1 mM). The membrane potential was held at −50 mV. The parameters are a mean ± S.E. of three independent measurements.

Substrate	I_{max}	$K_{0.5}$	$I_{max}/K_{0.5}$
	nA	*μM*	*nA / μM*
Gemcitabine	638 ± 58.1	59.7 ± 17.5	10.7
Ribavirin	546 ± 37.0	61.0 ± 13.2	9.0
AZT	420 ± 3.9	310 ± 9.0	1.4
3-Deazauridine	506 ± 29.8	50.8 ± 9.90	10.0

Pre–Steady-State Currents. Pre–steady-state currents were clearly demonstrated in each hCNT3 cRNA-injected oocyte during the voltage pulse processes under voltage-clamped conditions. The transient currents caused by the expression of hCNT3 with a slower decaying time constant were more noticeably observed in depolarizing testing membrane potentials than in hyperpolarizing membrane potentials during the voltage-jumping procedure (Figs. 5A and 6A). The pre–steady-state currents were almost completely abolished in the absence of sodium (100 mM *N*-methyl-D-glutamate chloride) in the perfusion buffer (Fig. 5B). The pre–steady-state currents also disappeared when 1.0 mM uridine (a substrate for this transporter) was applied in the presence of sodium (Fig. 5C). Pre–steady-state currents were not detected in water-injected oocytes (Fig. 5D).

The time constants (τ_2) for the pre–steady-state currents were voltage-dependent and were 4.7, 5.8, 10.3, 21.5, and 26.0 ms at testing membrane potentials of −150, −110, −70, −30, and 10 mV, respectively (Fig. 6B). The more depolarized the membrane potential, the larger the τ_2 values; at a testing membrane potential of ~10 mV, the τ_2 value reaches the maximum. In contrast, the time constant (τ_1) for the capacitive membrane currents was voltage-independent, ranging from 1.8 to 2.5 ms at all testing membrane potentials (Fig. 6B). The charge translocations at different voltages were fitted to the Boltzmann equation (see *Data Analysis of Electrophysiological Measurements*, above), and the relation between the charge transfer (Q) and the testing membrane potential showed a sigmoid pattern (Fig. 6C). The estimates of Q_{dep}, Q_{hyp}, z, and $V_{0.5}$ were 34.14 ± 8.23 nC, −11.38 ± 2.48

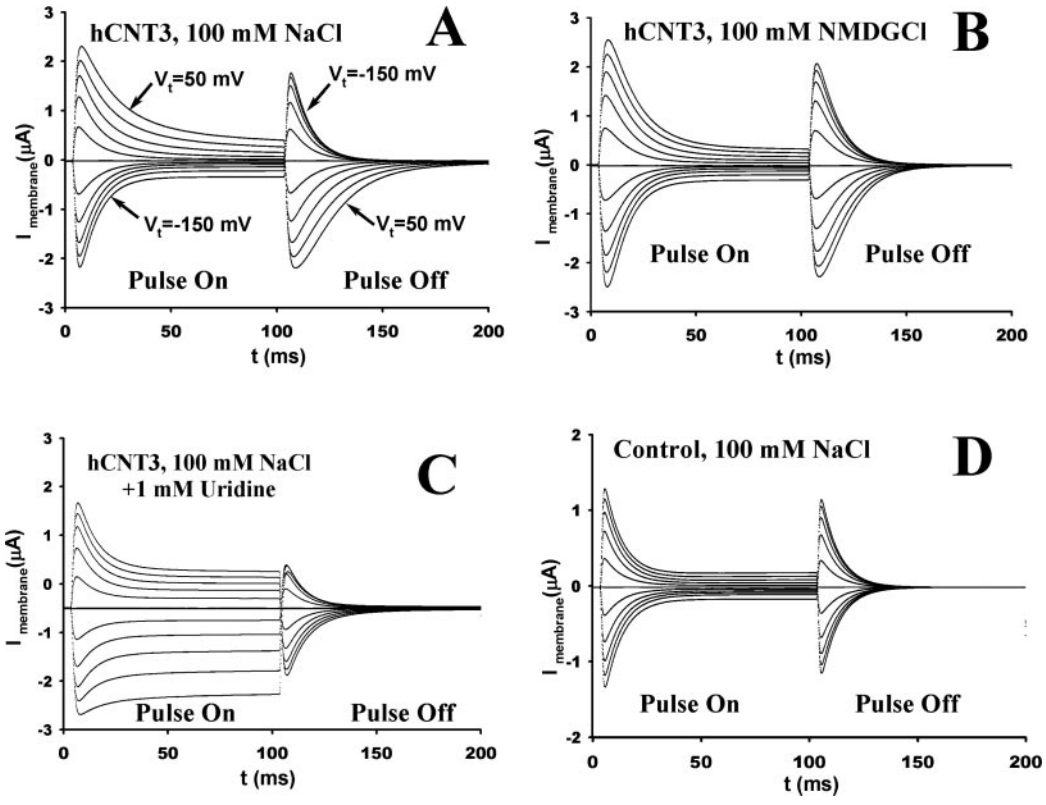

Fig. 5. Pre–steady-state currents in oocytes expressing hCNT3. Total membrane current curves during the pulse procedure in TEVC configuration in a representative hCNT3 cRNA-injected oocyte (A, B, and C) and a water-injected oocyte (D) under different conditions.

nC, 0.92 ± 0.33, and −9.28 ± 12.67 mV, respectively. The estimated maximal charge transfer (Q_{max}) was 45.5 nC.

Pharmacophore Models. The pharmacophore model generated using GASP revealed six important chemical features (Fig. 7D). Because three of them are donor site atom features (DS1, DS2, and DS3), which are proposed features originating at the transporter, only the remaining three features (Hydr1, AA1, and AA2) can be considered essential for molecules to be transported by hCNT3. AA1 signifies the importance of 3′-OH acting as H-bond acceptor, and AA2 represents the common ring oxygen atom serving as an H-bond acceptor atom. DS1 site atom feature is the inference of an H-bond donor atom from hCNT3 protein that may form a H-bond with the AA1 feature. Likewise, DS2 and DS3 are the two potential donor atoms from hCNT3 that may interact with AA2. Hydrophobic feature Hydr1 results from the alignment of the base rings, indicating the relative importance of an intact base ring structure at this position. DISCOtech pharmacophore model revealed similar requirements for hCNT3 transport (Fig. 7E). The presence of donor site DS2 indicates the requirement of ring oxygen for hCNT3 transport, which is present in all substrates with measured activities. Donor site DS1 and acceptor site AS1 both signify the importance of 3′-OH, complemented by acceptor atom AA1 and donor atom DA1. Analogous to GASP, the alignment of all base rings resulted in a hydrophobic center feature, Hydr1. Thus, both pharmacophore models identified three features that are necessary for hCNT3 transport: 1) the ring oxygen, 2) the 3′-OH moiety, and 3) the nucleobase ring. The interfeature distance requirements from both models are highly similar, as illustrated in Table 4.

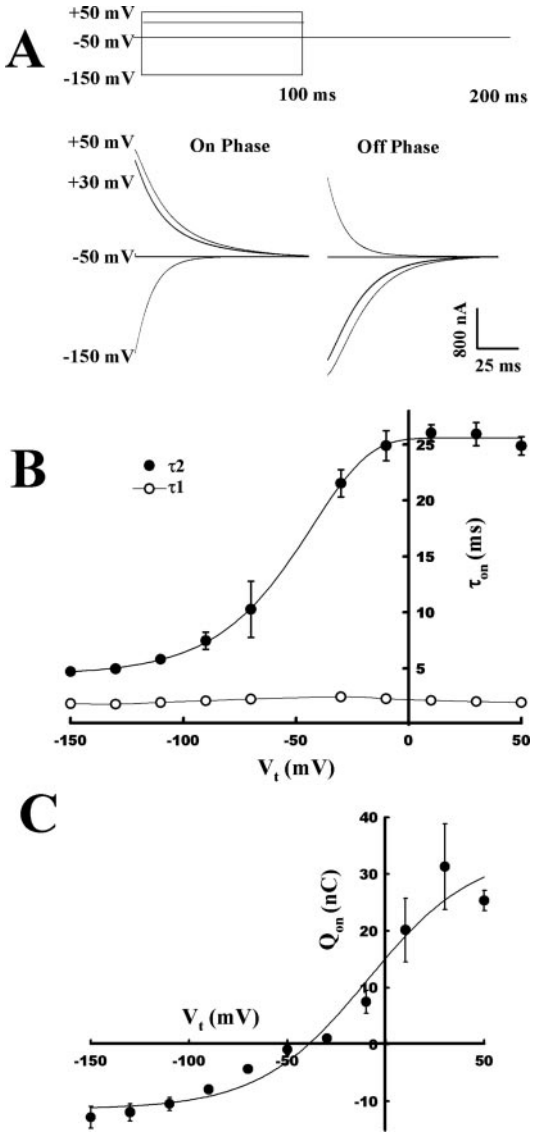

Fig. 6. Time constants of pre–steady-state currents and charge translocation in oocytes expressing hCNT3. A, representative carrier-mediated transient current curves (100 mM NaCl, pH 7.5) at testing membrane potentials of +50, +30, −50, and −150 mV, respectively, were obtained from the total currents by subtraction of the currents (I_1) due to membrane capacitance and the steady state currents (I_{ss}). Currents, filtered at 200 Hz for display, are also shown. B, the relaxation time constant (2 for the pre–steady-state currents is plotted as a function of the testing membrane potential. The relaxation time constant τ_1 for the capacitive membrane currents is also shown. C, charge (Q_{on}) translocation associated with hCNT3 expressed in oocytes as a function of the testing membrane potentials (V_t). Data are averages from three hCNT3 cRNA-injected oocytes in the absence of substrate.

3D-QSAR Models. Both CoMFA and CoMSIA models identified 6-azauridine as an outlier and it was excluded from further analyses. The standard CoMFA fields (i.e., electrostatic and steric interactions) show best correlation with hCNT3 substrate transport activity, yielding a traditional correlation coefficient (r^2) of 0.86 with 2 components. The statistical significance of the model was verified with a cross-validated correlation coefficient (q^2) of 0.63. Relative field contributions indicate that electrostatic interaction plays a more important role (72%) than steric interactions (28%) in the hCNT3 transport process. The statistical significance of both ComFA and CoMSIA models are listed in Table 5. CoMFA data can be further inspected by highlighting the respective field isocontours that significantly contribute to transport activity (Fig. 7B). The red contours (α, β) over the 3′-OH group indicate the importance of 3′-O for transportability, as do the blue contour (γ) over 3′-OH group for 3′-H and the green contour (δ) for the steric preference of 3′-OH group. All four contours signify the correlation of 3′-OH and hCNT3 transport. The blue contour (ϵ) below the 5(C)-position indicates the preference of more electropositive charge at this position by hCNT3. Whereas a more electropositive C(5) will enhance the transport by hCNT3, a more electronegative group will diminish the transport ability of the substrate. The yellow contour (ϕ) over 3(N)- specifies the potential for steric hindrance at this position. This is due to negative correlation at this position resulting from the methyl moiety in 1-methyl-adenosine. In general, bulky substitutions at this position should result in reduced transport by hCNT3. The influence of C(5) and N(3) modifications were previously noticed by Zhang et al. (2003); however, our computational analysis provides higher resolution to determine subtle correlations at these two. Furthermore, we were able to identify additional positions that contribute to hCNT3 transport.

The CoMSIA study revealed that H-bond acceptor fields correlated best with hCNT3 substrate affinity (r^2, 0.80; q^2, 0.62; three components). Visual inspection of the top 20% correlations between H-bond acceptor fields and transport activities (Fig. 7C) revealed a purple contour (α) over 3′-OH, reaffirming the necessity of 3′-OH in hCNT3 transport as an H-bond acceptor. On the other hand, the yellow contour (β) over 2′-OH indicates the insignificance of 2′-OH to the transport by hCNT3. Another yellow contour γ over the 5(C)-

position reveals that H-bond formation with an acceptor at this position is not essential for hCNT3 transport.

Discussion

In this study, we expressed hCNT3 in *X. laevis* oocytes and examined the Na^+-dependent substrate-induced inward currents using a two-microelectrode voltage-clamp technique. In addition, only substrate-induced currents are detected by this method, which eliminates any confounding contribution of potentially high degree of substrate diffusion via a noncarrier-mediated process to the intracellular accumulation of substrate. This is especially important for compounds that have high membrane permeability (e.g., AZT).

Because hCNT3 is a sodium-dependent cotransporter and its substrates are electrically neutral, the Na^+-substrate cotransport is electrogenic. Therefore, the transporter function can be monitored by substrate-induced inward currents in the presence of Na^+. In addition, H^+-dependent activation of hCNT3 has been observed (Smith et al., 2005), although the transport activity is relatively minor compared with that observed after Na^+-activation. These experiments showed that the transport of gemcitabine by hCNT3 occurs with a Na^+/gemcitabine stoichiometry of 2:1 and that the Na^+-activation kinetics is independent of membrane potential. This Na^+/gemcitabine stoichiometry of 2:1 is consistent with the Na^+/uridine stoichiometry reported by Smith et al. (2005) or that determined by Hill analysis in *X. laevis* oocytes (Ritzel et al., 2001). Furthermore, for gemcitabine transport, neither the sodium affinity constant ($K_{0.5}$) nor the translocation ratio was dependent on membrane potential, confirming that the Na^+/substrate translocation ratio remains constant. Our estimate of the $K_{0.5}$ of Na^+ activation (8 mM) is also comparable with that observed by other investigators (Ritzel et al., 2001; Smith et al., 2005). These data suggest that the kinetics of Na^+-activation of hCNT3 transport is independent of the substrate (i.e., uridine or gemcitabine).

We characterized the transport kinetics of the six major naturally occurring nucleosides by analysis of Na^+-dependent inward currents induced by these compounds. Our $K_{0.5}$ and $I_{max}/K_{0.5}$ ratios are in relatively close agreement with the K_m and V_{max}/K_m ratios obtained by radiolabeled transport assays with hCNT3 expressed in *X. laevis* oocytes (Ritzel et al., 2001), Cos7L cells (Toan et al., 2003), and *Saccharomyces cerevisiae* (Zhang et al., 2003), further suggesting that measuring the Na^+-dependent substrate-induced currents is a valid method to study substrate transport kinetics for this electrogenic transporter.

Next, we measured the kinetics of transport of nucleoside drugs. We observed that both I_{max} and $K_{0.5}$ of gemcitabine, ribavirin, AZT, and 3-deazauridine were dependent on membrane potential. In contrast, the $K_{0.5}$ for gemcitabine, uri-

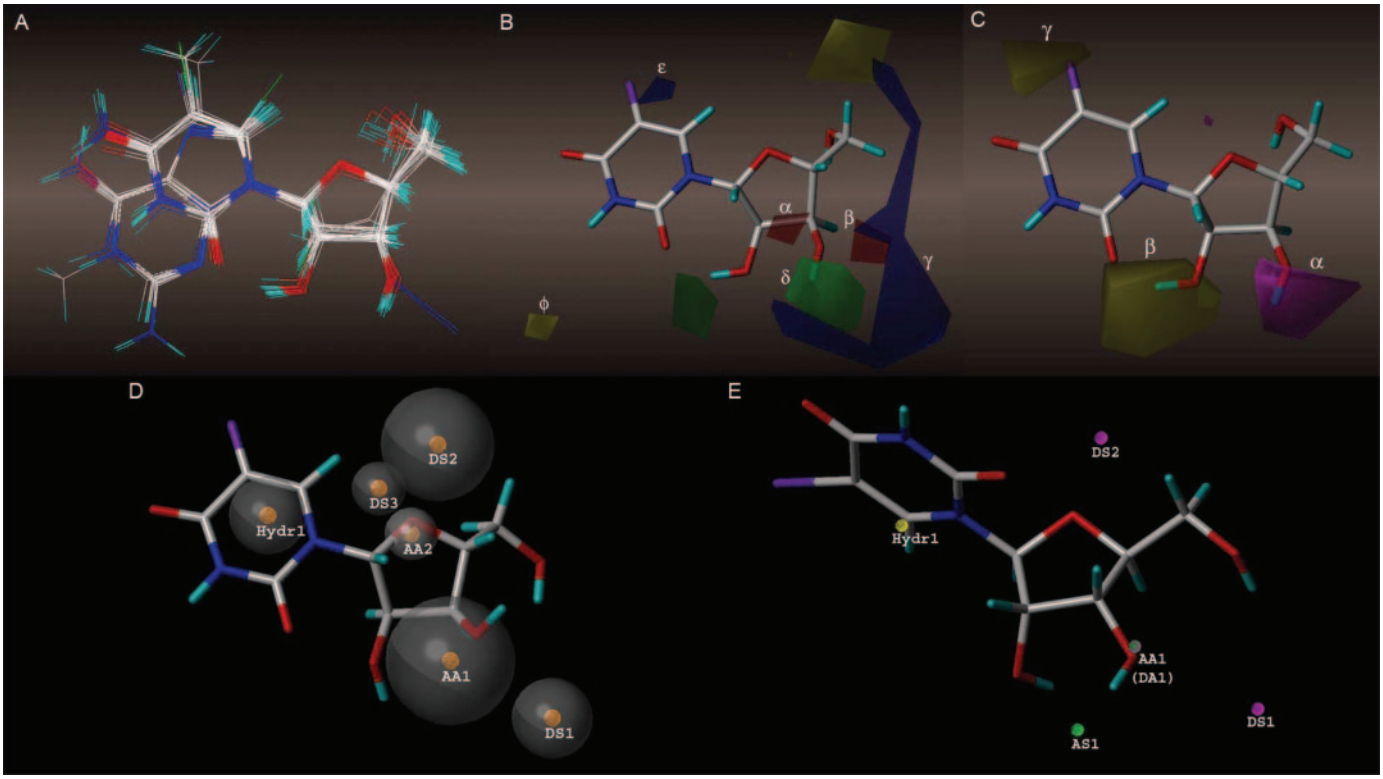

Fig. 7. Transport 3D-QSAR and pharmacophore models for hCNT3. A, overall alignment of 32 hCNT3 substrates (6-azauridine excluded) with measured transport activities. B, CoMFA coefficient contours surrounding the substrate with highest transport activity (5-iodouridine) illustrating the correlation of electrostatic and steric fields with transport activity. Steric contour maps indicate that higher affinity for transport is correlated with less steric bulk near yellow contours and more steric near green. Electrostatic contours suggest that more negative electrostatic charge near red and more positive charge near blue will increase hCNT3 transport. C, CoMSIA coefficient contour map surrounding 5-iodouridine illustrating the correlation of H-bond acceptor fields with transport activity. Purple contours signify positive correlation between H-bond acceptor at that position and hCNT3 transportability, whereas yellow contours indicate the insignificance of the H-bond acceptor at that position for hCNT3 transportability. D, transport pharmacophore model for hCNT3 generated by GASP. Yellow spheres represent chemical features, and the radii of gray spheres illustrate the tolerance of each feature. Hydr, hydrophobic feature; AA, acceptor atom feature; DS, donor site feature. E, transport pharmacophore model for hCNT3 generated by DISCOtech. Spheres with different colors represent chemical features. AS, acceptor site feature.

dine, and 5′-deoxy-5-fluorouridine for hCNT1 expressed in *X. laevis* oocytes were independent of membrane potential (Larrayoz et al., 2004). This suggests that hyperpolarization alters the conformation of the transporter to decrease substrate affinity of hCNT3 but not hCNT1. We observed a membrane potential dependent I_{max} for gemcitabine and the uridine analog 3-deazauridine similar to that observed for uridine in hCNT1. In contrast, the hCNT1 I_{max} of gemcitabine is independent of membrane potential (Larrayoz et al., 2004). This difference in the membrane potential dependence of gemcitabine I_{max} may be due to a difference in the rate-limiting steps in gemcitabine transport between hCNT3 and hCNT1.

Both AZT and 2′,3′-dideoxyinosine have recently been shown to be low-affinity/high-capacity substrates of hCNT1 (Cano-Soldado et al., 2004). Our data show for the first time that AZT is also a low-affinity/high-capacity substrate of hCNT3 with an apparent affinity ($K_{0.5}$) of 310 μM and an $I_{max}/K_{0.5}$ ratio approximately 10-fold lower than the average of the six natural nucleosides that we examined. Previous data on whether hCNT3 is capable of AZT transport have been contradictory. Uridine or thymidine transport by both hCNT3-overexpressing Cos7L cells (Toan et al., 2003) and rat MLS-9 (microglial) cells expressing the cib type transporter (Hong et al., 2000) was sensitive to inhibition at the high concentration of 2 and 1 mM AZT, respectively. This is in contrast to previous published reports in which the estimated K_i of AZT (determined by inhibition of radiolabeled uridine transport) for hCNT3 expressed in *S. cerevisiae* was reported to be greater than 2 mM (Zhang et al., 2003). This difference may be due to differences in the yeast recombinant expression system, because our data in *X. laevis* oocytes and that observed from mammalian cell lines are in agreement. The azido group of the 3′-position of the ribose ring contributes to the relatively high lipophilicity (log P_{oct} 0.13) of AZT (Bergstrom et al., 2003), and depending on the level of nucleoside transporter expression, the diffusional component of AZT uptake can potentially be greater than the transporter-mediated component of AZT transport. Nevertheless, our data suggest that hCNT3 does indeed play a role in AZT transport and that AZT could potentially inhibit the hCNT3-mediated transport of other substrates.

Significant pre–steady-state or transient currents in the hCNT3-expressing oocytes were observed during our electrophysiology studies using a two-electrode, voltage-clamp configuration. The transient currents caused by charge movements associated with the hCNT3 expression in the absence of substrates have the following features. The transient currents were observed only in the hCNT3-expressing oocytes, whereas they were not observed in water-injected control oocytes, indicating that the currents were a result of hCNT3 expression. The charge translocation was completely eliminated by an hCNT3-specific substrate, uridine, at a saturating concentration (1 mM), and the charge movement was also dependent on the presence of Na^+. In addition, the charge movement (Q) seemed to be saturated at extremely hyperpolarizing or depolarizing membrane potentials, and its reversal point occured at or near the holding membrane potential (V_h, ~−50 mV, Fig. 6C). The value of Q_{max} (45.5 nC) reflects the transporter density within the plasma membrane of the hCNT3-expressing oocytes. The ratio of the maximal substrate-induced steady-state current, I_{max} (~1560 nA at −150 mV, data not shown), versus the maximal charge movement, Q_{max}, indicates the apparent turnover rate ($k = I_{max}/Q_{max}$) for the translocation of the substrate-bound transporters from the external to the internal surfaces of the oocyte plasma membrane. The estimated turnover number (k) of the transporter hCNT3 expressed in *X. laevis* oocytes was 34 s^{-1}.

To determine the structure-activity relationship of hCNT3, we used a two-microelectrode voltage-clamp system to determine the ability of a large panel of nucleoside analogs to induce inwardly directed currents by hCNT3 expressed in *X. laevis* oocytes. This system directly measures the transport of the various nucleoside analogs. When radiolabeled nucleoside analogs are not readily available for direct transport measurements, the alternative strategy is to measure the inhibition of a radiolabeled probe substrate (e.g., [^{3}H]uridine) in the presence of various unlabeled nucleoside analog inhibitors (Zhang et al., 2003). This method interprets inhibition of the probe substrate transport by the various nucleoside analogs as an indication that the analog is also a substrate of the transporter. This assumption may not always be correct. For example, a compound may inhibit the transport of a radiolabeled probe substrate, but the compound itself may not be translocated. The electrophysiological approach used in the present study provides a method to differentiate between an inhibitor and a competing substrate. If a compound induces inwardly directed currents in a Na^+-dependent manner in oocytes expressing an electrogenic transporter, such

TABLE 4
Intramolecular atomic distances (Å) between pharmacophoric feature points

	AA1	Hydr1	AA2	DS1	DS2	DS3
GASP						
Hydr1	5.61		3.46	8.37	4.67	3.89
AA1			3.28	2.8	5.27	5.57
AA2				5.62	2.86	2.86
DS1					7.15	7.67
DS2						4.67
DISCOtech						
AA1 (DA1)		5.92	2.9	2.9	5.93	
Hydr1			7.13	8.42	4.74	
AS1				4.57	8.55	
DS1					7.28	

Hydr, hydrophobic feature; AA, acceptor atom feature; DA, donor atom feature; DS, donor site feature; AS, acceptor site feature.

TABLE 5
3D-QSAR modeling statistics for hCNT3

	q^2	Press	r^2	s	No.[a]	% Steric	% Electrostatic	Outliers[b]
CoMFA	0.63	17.6	0.86	10.76	2	28	72	1
CoMSIA	0.62	18.0	0.80	13.01	3	0	100[c]	1

[a] Number of components used for non–cross-validated analyses.
[b] 6-Azauridine was identified as an outlier and not included in the analysis.
[c] H-bond acceptor field.
q^2, cross-validated correlation coefficient; r^2, traditional (non-cross-validated) correlation coefficient.

data can be interpreted as direct evidence for translocation of the compound by the transporter.

Our data also suggest that, for hCNT3, the 3′-hydroxyl on the ribose is a critical determinant in substrate specificity. The exceptions are 3′-deoxy- and 2′,3′-dideoxyuridine, both of which stimulated substantial Na^+-dependent inward current. The latter is in contrast to inhibition data with hCNT3 expressed in *S. cerevisiae*, where the K_i of 3′-deoxyuridine for hCNT3 was estimated to be 258 μM, and no inhibition of [^{3}H]uridine transport was observed by 2 mM 2′,3′-dideoxyuridine (Zhang et al., 2002). As observed with AZT, the yeast system seems to be discrepant with the *X. laevis* oocyte expression system. Thus, this difference is likely to be due to differences in the expression system used.

Two independent pharmacophore models identified the same binding requirements for hCNT3, ring oxygen, 3′-OH, and base ring. We compared these models with previously generated nucleoside transporter pharmacophore models for hCNT1, hCNT2, and hENT1 (Chang et al., 2004). We noticed less stringent substrate requirements for hCNT3 compared with hCNT1 and hCNT2, which require an additional H-bond acceptor feature on the base ring; however, substrate requirements are similar to hENT1 pharmacophore model, which requires only a sugar ring, 3′-OH, and a nucleobase ring. This observation is consistent with the fact that hCNT3 exhibits broad nucleoside substrate selectivity, capable of transporting both purines and pyrimidines, characteristic of hENT1, but distinctly different from hCNT1 and hCNT2, which selectively transport pyrimidines and purines, respectively.

In addition to pharmacophore modeling, we applied 3D-QSAR, a more quantitative approach, to further correlate measured transport activities with specific functional groups or regions on the nucleoside molecule. Whereas the CoMFA algorithm correlated electrostatic and steric interactions with hCNT3 transport activity, CoMSIA additionally implicated the role of H-bond interactions in hCNT3 transport process. Both approaches were validated with robust statistics, and their elucidation of hCNT3 transporter-substrate interactions was mutually consistent and complementary. Other than identifying the 3′-OH group as an important hCNT3 transport determinant, both models revealed structural features on the base ring that correlated with hCNT3 transportability. We have generated 3D-QSAR models for hCNT1, hCNT2, and hENT1 (Chang et al., 2004), which provides an excellent opportunity to compare the four nucleoside transporters. The hCNT3 substrate structural requirement for a sugar ring is similar to that of hENT1, which requires only a 3′-OH. It is noteworthy that both pharmacophore modeling and experimental observation reaffirm this feature. The structural requirements for the base ring, however, are more subtle and can be used to effectively distinguish between the different nucleoside transporters. For example, hCNT3 prefers electropositive charge at the 5-position and absence of bulky substituents at the 3-position of the pyrimidine ring; hCNT1 favors more positive charge surrounding the 3,6-position of the pyrimidine ring; hCNT2 prefers hydrogen bond formation at the 2-position; and hENT1 favors a negative charge at the 3,4,5-position of pyrimidine ring. However, it is important to note that these conclusions are drawn from two different methods of generating experimental data. Whereas the current model is derived from transport data, the previous models were based on inhibition data. Thus, care should be taken in extrapolating the aforementioned general structural requirements until transport data can be used for generating pharmacophore and 3D-QSAR model for hCNT1, hCNT2, and hENT1.

In summary, we have characterized in detail the structure-activity relationship and the electrophysiology of hCNT3 in the *X. laevis* oocyte expression system. Our results highlight the utility of electrophysiological analysis for rapid and high-sensitivity characterization of the kinetic behavior of the transport of nucleoside substrates by hCNT3. In addition, the discrepancies in results obtained from transport studies using radiolabeled AZT compared with AZT-stimulated inward currents highlight the effects that the diffusional component of hydrophobic substrates may have on the interpretation of uptake data with radiolabeled substrates.

Acknowledgments

We thank Dr. Yurong Lai for assistance in cloning hCNT3.

References

Baldwin SA, Beal PR, Yao SY, King AE, Cass CE, and Young JD (2004) The equilibrative nucleoside transporter family, SLC29. *Pflueg Arch Eur J Physiol* **447:**735–743.

Bergstrom CA, Strafford M, Lazorova L, Avdeef A, Luthman K, and Artursson P (2003) Absorption classification of oral drugs based on molecular surface properties. *J Med Chem* **46:**558–570.

Boorer KJ, Loo DD, and Wright EM (1994) Steady-state and presteady-state kinetics of the H^+/hexose cotransporter (STP1) from Arabidopsis thaliana expressed in *Xenopus* oocytes. *J Biol Chem* **269:**20417–20424.

Cano-Soldado P, Lorrayoz IM, Molina-Arcas M, Casado FJ, Martinez-Picado J, Lostao MP, and Pastor-Anglada M (2004) Interaction of nucleoside inhibitors of HIV-1 reverse transcriptase with the concentrative nucleoside transporter-1 (SLC28A1). *Antivir Ther* **9:**993–1002.

Chang C, Swaan PW, Ngo LY, Lum PY, Patil SD, and Unadkat JD (2004) Molecular requirements of the human nucleoside transporters hCNT1, hCNT2 and hENT1. *Mol Pharmacol* **65:**558–570.

Gray JH, Owen RP, and Giacomini KM (2004) The concentrative nucleoside transporter family, SLC28. *Pflueg Arch Eur J Physiol* **447:**728–734.

Hong M, Schlichter L, and Bendayan R (2000) A Na^+-dependent nucleoside transporter in microglia. *J Pharmacol Exp Ther* **292:**366–374.

Horwitz JP, Massova I, Wiese TE, Besler BH, and Corbett TH (1994) Comparative molecular field analysis of the antitumor activity of 9H-thioxanthen-9-one derivatives against pancreatic ductal carcinoma 03. *J Med Chem* **37:**781–786.

Huang Y, Anderle P, Bussey KJ, Barbacioru C, Shankavaram U, Dai Z, Reinhold WC, Papp A, Weinstein JN, and Sadee W (2004) Membrane transporters and channels: role of the transportome in cancer chemosensitivity and chemoresistance. *Cancer Res* **64:**4294–4301.

Jarvis SM, Thorn JA, and Glue P (1998) Ribavirin uptake by human erythrocytes and the involvement of nitrobenzylthioinosine-sensitive (es)-nucleoside transporters. *Br J Pharmacol* **123:**1587–1592.

Jones G, Willett P, and Glen RC (1995) A genetic algorithm for flexible molecular overlay and pharmacophore elucidation. *J Comput Aided Mol Des* **9:**532–549.

Kong W, Engel K, and Wang J (2004) Mammalian nucleoside transporters. *Curr Drug Metab* **5:**63–84.

Kroemer RT, Koutsilieri E, Hecht P, Liedl KR, Riederer P, and Kornhuber J (1998) Quantitative analysis of the structural requirements for blockade of the *N*-methyl-D-aspartate receptor at the phencyclidine binding site. *J Med Chem* **41:**393–400.

Lai Y, Lee EW, Ton CC, Vijay S, Zhang H, and Unadkat JD (2005) Conserved residues F316 and G476 in the concentrative nucleoside transporter 1 (hCNT1) affect guanosine sensitivity and membrane expression, respectively. *Am J Physiol* **288:**C39–C45.

Lai Y, Tse CM, and Unadkat JD (2004) Mitochondrial expression of the human equilibrative nucleoside transporter 1 (hENT1) results in enhanced mitochondrial toxicity of antiviral drugs. *J Biol Chem* **279:**4490–4497.

Larrayoz IM, Casado FJ, Pastor-Anglada M, and Lostao MP (2004) Electrophysiological characterization of the human Na^+/nucleoside cotransporter 1 (hCNT1) and role of adenosine on hCNT1 function. *J Biol Chem* **279:**8999–9007.

Loo DD, Hazama A, Supplisson S, Turk E, and Wright EM (1993) Relaxation kinetics of the Na^+/glucose cotransporter. *Proc Natl Acad Sci USA* **90:**5767–5771.

Lum PY, Ngo LY, Bakken AH, and Unadkat JD (2000) Human intestinal es nucleoside transporter: molecular characterization and nucleoside inhibitory profiles. *Cancer Chemother Pharmacol* **45:**273–278.

Mackenzie B, Fei YJ, Ganapathy V, and Leibach FH (1996a) The human intestinal H^+/oligopeptide cotransporter hPEPT1 transports differently-charged dipeptides with identical electrogenic properties. *Biochim Biophys Acta* **1284:**125–128.

Mackenzie B, Loo DD, Fei Y, Liu WJ, Ganapathy V, Leibach FH, and Wright EM (1996b) Mechanisms of the human intestinal H^+-coupled oligopeptide transporter hPEPT1. *J Biol Chem* **271:**5430–5437.

Mackey JR, Mani RS, Selner M, Mowles D, Young JD, Belt JA, Crawford CR, and

Cass CE (1998) Functional nucleoside transporters are required for gemcitabine influx and manifestation of toxicity in cancer cell lines. *Cancer Res* **58:**4349–4357.
Mangravite LM, Badagnani I, and Giacomini KM (2003) Nucleoside transporters in the disposition and targeting of nucleoside analogs in the kidney. *Eur J Pharmacol* **479:**269–281.
Martin YC, Bures MG, Danaher EA, DeLazzer J, Lico I, and Pavlik PA (1993) A fast new approach to pharmacophore mapping and its application to dopaminergic and benzodiazepine agonists. *J Comput Aided Mol Des* **7:**83–102.
Mata JF, Garcia-Manteiga JM, Lostao MP, Fernandez-Veledo S, Guillen-Gomez E, Larrayoz IM, Lloberas J, Casado FJ, and Pastor-Anglada M (2001) Role of the human concentrative nucleoside transporter (hCNT1) in the cytotoxic action of 5[prime]-deoxy-5-fluorouridine, an active intermediate metabolite of capecitabine, a novel oral anticancer drug. *Mol Pharmacol* **59:**1542–1548.
Panayotova-Heiermann M, Loo DD, and Wright EM (1995) Kinetics of steady-state currents and charge movements associated with the rat Na^+/glucose cotransporter. *J Biol Chem* **270:**27099–27105.
Parent L, Supplisson S, Loo DD, and Wright EM (1992) Electrogenic properties of the cloned Na^+/glucose cotransporter: II. A transport model under nonrapid equilibrium conditions. *J Membr Biol* **125:**63–79.
Patil SD, Ngo LY, Glue P, and Unadkat JD (1998) Intestinal absorption of ribavirin is preferentially mediated by the Na^+-nucleoside purine (N1) transporter. *Pharm Res (NY)* **15:**950–952.
Patil SD, Ngo LY, and Unadkat JD (2000) Structure-inhibitory profiles of nucleosides for the human intestinal N1 and N2 Na^+-nucleoside transporters. *Cancer Chemother Pharmacol* **46:**394–402.
Ritzel MW, Ng AM, Yao SY, Graham K, Loewen SK, Smith KM, Ritzel RG, Mowles DA, Carpenter P, Chen XZ, et al. (2001) Molecular identification and characterization of novel human and mouse concentrative Na^+-nucleoside cotransporter proteins (hCNT3 and mCNT3) broadly selective for purine and pyrimidine nucleosides (system cib). *J Biol Chem* **276:**2914–2927.
Schaal W, Karlsson A, Ahlsen G, Lindberg J, Andersson HO, Danielson UH, Classon B, Unge T, Samuelsson B, Hulten J, et al. (2001) Synthesis and comparative molecular field analysis (CoMFA) of symmetric and nonsymmetric cyclic sulfamide HIV-1 protease inhibitors. *J Med Chem* **44:**155–169.
Smith KM, Slugoski MD, Loewen SK, Ng AM, Yao SY, Chen XZ, Karpinski E, Cass CE, Baldwin SA, and Young JD (2005) The broadly selective human Na^+/nucleoside cotransporter (hCNT3) exhibits novel cation-coupled nucleoside transport characteristics. *J Biol Chem* **280:**25436–25449.
Swaan PW, Szoka FC Jr, and Oie S (1997) Molecular modeling of the intestinal bile acid carrier: a comparative molecular field analysis study. *J Comput Aided Mol Des* **11:**581–588.
Toan SV, To KK, Leung GP, de Souza MO, Ward JL, and Tse CM (2003) Genomic organization and functional characterization of the human concentrative nucleoside transporter-3 isoform (hCNT3) expressed in mammalian cells. *Pflueg Arch Eur J Physiol* **447:**195–204.
Zhang J, Visser F, Vickers MF, Lang T, Robins MJ, Nielsen LP, Nowak I, Baldwin SA, Young JD, and Cass CE (2003) Uridine binding motifs of human concentrative nucleoside transporters 1 and 3 produced in Saccharomyces cerevisiae. *Mol Pharmacol* **64:**1512–1520.
Zhang JL, Simeonowa I, Wang Y, and Sebald W (2002) The high-affinity interaction of human IL-4 and the receptor alpha chain is constituted by two independent binding clusters. *J Mol Biol* **315:**399–407.

Address correspondence to: Dr. Jashvant D. Unadkat, Department of Pharmaceutics, Box 357610, University of Washington, Seattle, WA 98195. E-mail: jash@u.washington.edu